


FULL PAPER

Open Access



# Repeated triggered ruptures on a distributed secondary fault system: an example from the 2016 Kumamoto earthquake, southwest Japan

Daisuke Ishimura<sup>1\*</sup> , Hiroyuki Tsutsumi<sup>2</sup>, Shinji Toda<sup>3</sup>, Yo Fukushima<sup>3</sup>, Yasuhiro Kumahara<sup>4</sup>, Naoya Takahashi<sup>5</sup>, Toshihiko Ichihara<sup>6</sup> and Keita Takada<sup>7</sup>

## Abstract

The Mw7.0 2016 Kumamoto earthquake occurred on the previously mapped Futagawa–Hinagu fault causing significant strong ground motions. A ~30-km-long dextral surface rupture appeared on the major fault zone and dextral slip was up to 2–3 m. However, the surface ruptures were also broadly and remotely distributed approximately 10 km away from the primary rupture zone. These numerous distributed secondary surface slips with vertical displacement of less than a few tens of centimeters were detected by the interferometric synthetic aperture radar (InSAR) technology in previous studies. Such displacements occurred not only on previously mapped faults but also on unknown traces. Here, we addressed the following fundamental issues: whether the broadly distributed faults were involved in the past major earthquakes in the neighborhood, and how the fault topography of such secondary faults develops, seismically or aseismically. To find clues for understanding these issues, we show the results of field measurements of surface slips and paleoseismic trenching on distributed secondary faults called the Miyaji faults inside the Aso caldera, 10 km away from the eastern end of the primary rupture zone. Field observations revealed small but well-defined dextral slip surface ruptures that were consistent with vertical and dextral offsets derived from InSAR. On the trench walls, the penultimate event with vertical displacements almost similar to the 2016 event was identified. The timing of the penultimate event was around 2 ka, which was consistent with that of the primary fault and archeological information of the caldera. Considering the paleo-slip event and fault models of the Miyaji faults, they were presumed not to be source faults, and slip on these faults have been triggered by large earthquakes along major adjacent active faults. The results provide important insights into the seismic hazard assessment of low-slip-rate active faults and fault topography development due to triggered displacement along secondary faults.

**Keywords:** 2016 Kumamoto earthquake, Surface rupture, Trench excavation, Low-slip-rate active fault, Secondary fault, Tephra, Aso caldera, InSAR

## Introduction

Seismic-related high-resolution surface displacements (less than 10 cm) have been detected worldwide by recent satellite geodetic observations. Notably, interferometric synthetic aperture radar (InSAR) revealed that slips occurred off the fault primarily responsible for earthquakes (hereinafter, primary fault) and facilitated the understanding of tectonic geomorphology (e.g., Price

\*Correspondence: [ishimura@tmu.ac.jp](mailto:ishimura@tmu.ac.jp)

<sup>1</sup> Department of Geography, Tokyo Metropolitan University, 1-1, Minami-Osawa, Hachioji, Tokyo 192-0397, Japan

Full list of author information is available at the end of the article

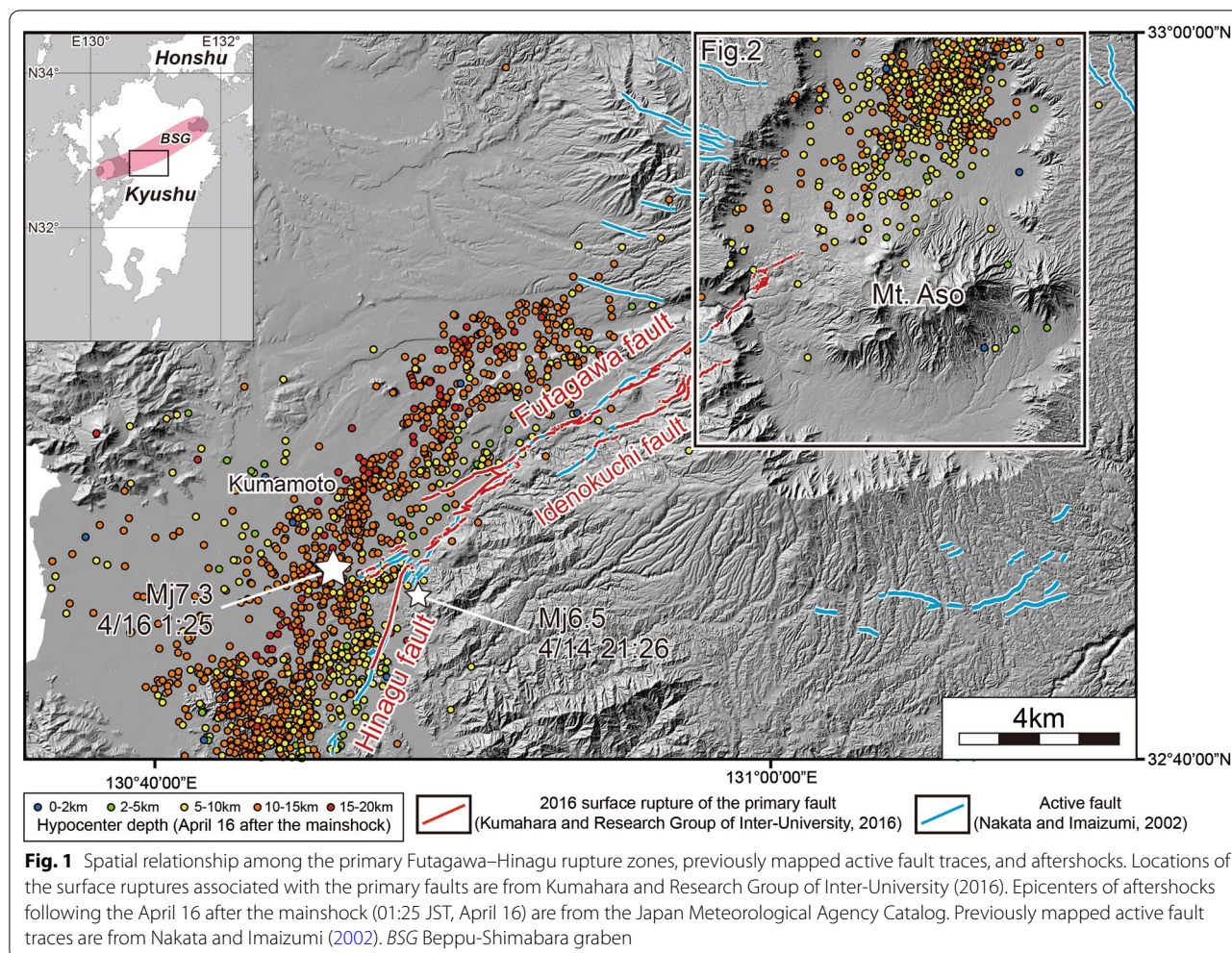
and Sandwell 1998; Wright et al. 2001; Fialko et al. 2002; Nishimura et al. 2008; Wei et al. 2011; Fujiwara et al. 2016). These recent studies have suggested that secondary surface ruptures were ubiquitous phenomena, contributing to the accumulation of displacements on faults away from the primary fault. During the 2016 Kumamoto earthquake sequence, many distributed secondary surface ruptures with a few to tens of centimeters scale displacements appeared in the areas around the primary fault (Fujiwara et al. 2016; Toda et al. 2016; Goto et al. 2017). The 2016 Kumamoto earthquake emphasized the significance of understanding the activity and development of secondary faults. If such displacement is triggered whenever the primary fault ruptures, several issues arise for the assessment of secondary faults. Triggered displacements contribute to fault topography development and lead to an overestimation of the slip rates, which represent the seismogenic activity of the secondary faults. Their recurrence intervals revealed by paleoseismic studies include both the triggered slips and seismogenic events. The risks of displacement hazards of secondary faults may increase in terms of frequency (Toda and Ishimura 2019).

On the other hand, consideration of such triggered slip on faults off primary faults provides new insights into the behavior of low-slip-rate active faults (hereinafter, LSRAF). The behavior of LSRAFs has been a problem of the seismic hazard assessment in Japan due to the following two issues. One problem is related to the detectivity level of LSRAFs. Asada (1991) has already pointed out the discrepancy between the number of LSRAFs and their expected number from large inland earthquakes by considering fault slip rates. Considering the relationship between the slip rates and recurrence intervals, Asada (1991) claimed that the number of LSRAFs should be much higher than the number of high-slip-rate active faults (hereinafter, HSRAFs). However, there are not many mapped LSRAFs against the HSRAFs in Japan (Research Group for Active Faults of Japan 1980, 1991; Nakata and Imaizumi 2002; Imaizumi et al. 2018). This indicates that most LSRAFs have not been detected due to the oversight and/or erosion and sedimentation that have removed tectonic geomorphic features. Therefore, it was noted that short-length and/or low-slip-rate active faults are also important for seismic hazards assessment. Shimazaki (2008) pointed out that the magnitude of such short-length active faults except for volcanic area is  $M_j$  6.9 or larger based on reports on large shallow crustal earthquakes in Japan.

The other is the slip characteristic of LSRAFs. Since the March 11, 2011 Tohoku-oki earthquake ( $M_w$  9.0), the surface ruptures associated with the inland earthquakes have appeared in Fukushima (Maruyama et al.

2014; Toda and Tsutsumi 2013; Miyashita 2018), Ibaraki (Fukushima et al., 2018; Komura et al., 2019), Nagano (e.g., Okada et al. 2015; Ishimura et al. 2019), and Kumamoto (e.g., Shirahama et al. 2016; Toda et al. 2016; Goto et al. 2017) prefectures in Japan. Among them, the events involving slips on LSRAFs are Fukushima, Ibaraki, and Kumamoto cases. In these cases, there were two types of LSRAF behaviors; some of them were seismogenic, others were not. As examples of the former, the April 11, 2011 earthquake ( $M_w$  6.6) in the Fukushima Prefecture, and the March 19, 2011 and December 28, 2016 earthquakes ( $M_w$  5.8 and 5.9, respectively) in Ibaraki Prefecture occurred along LSRAFs (Maruyama et al. 2014; Toda and Tsutsumi 2013; Miyashita 2018; Fukushima et al. 2018; Komura et al. 2019). The 2011 Fukushima earthquake occurred along the previously mapped Itozawa and Yunodake faults. The vertical slip rate of the Itozawa fault was estimated to be less than 0.07 mm/yr (Maruyama et al. 2014). The 2011 and 2016 Ibaraki events occurred along a previously unmapped active fault, and its vertical slip rate was roughly estimated not exceeding 0.1 mm/yr based on the geomorphic features and denudation rate (Komura et al. 2019). In addition, it has been suggested that the sudden stress changes caused by massive deformations during and after the 2011 Tohoku-oki earthquake triggered these earthquakes (Fukushima et al. 2018). An example of the latter case is the 2016 Kumamoto earthquake sequence. The mainshock occurred along the mapped Futagawa–Hinagu fault (Fig. 1) but simultaneously caused slips in the adjacent mapped and unmapped active faults (Fujiwara et al. 2016), contributing to the development of fault topography. Vertical slip rates of the mapped active faults where secondary surface ruptures appeared were estimated to be approximately 0.1 mm/yr (Research Group for Active Faults of Japan 1991) and thus those of the unmapped active faults are also probably classified to be LSRAFs due to the threshold of detectivity of active faults in the region. These recent examples highlighted a question on the slip characteristics of LSRAFs. Therefore, paleoseismic studies on LSRAFs of which detailed locations are known can provide insights for understanding their complications.

In this study, to understand the characteristics of LSRAFs, we focused on the relationship between the primary and secondary faults that ruptured during the  $M_w$  7.0 April 16, 2016 event (the mainshock of the Kumamoto earthquake sequence). We conducted field measurements of surface slips and paleoseismic trenching on small secondary surface ruptures (< 10 cm displacement) 10 km away from the surface ruptures along the primary fault, i.e., the Futagawa fault. In addition, in combination with InSAR analysis, field measurements of displacements were compared with InSAR-derived 3D



displacement data in both vertical and horizontal (fault-parallel) directions, and the subsurface structures were discussed. The details of the InSAR analysis and fault slip inversion were shown in Fukushima and Ishimura (2020), which is a partner study with this study.

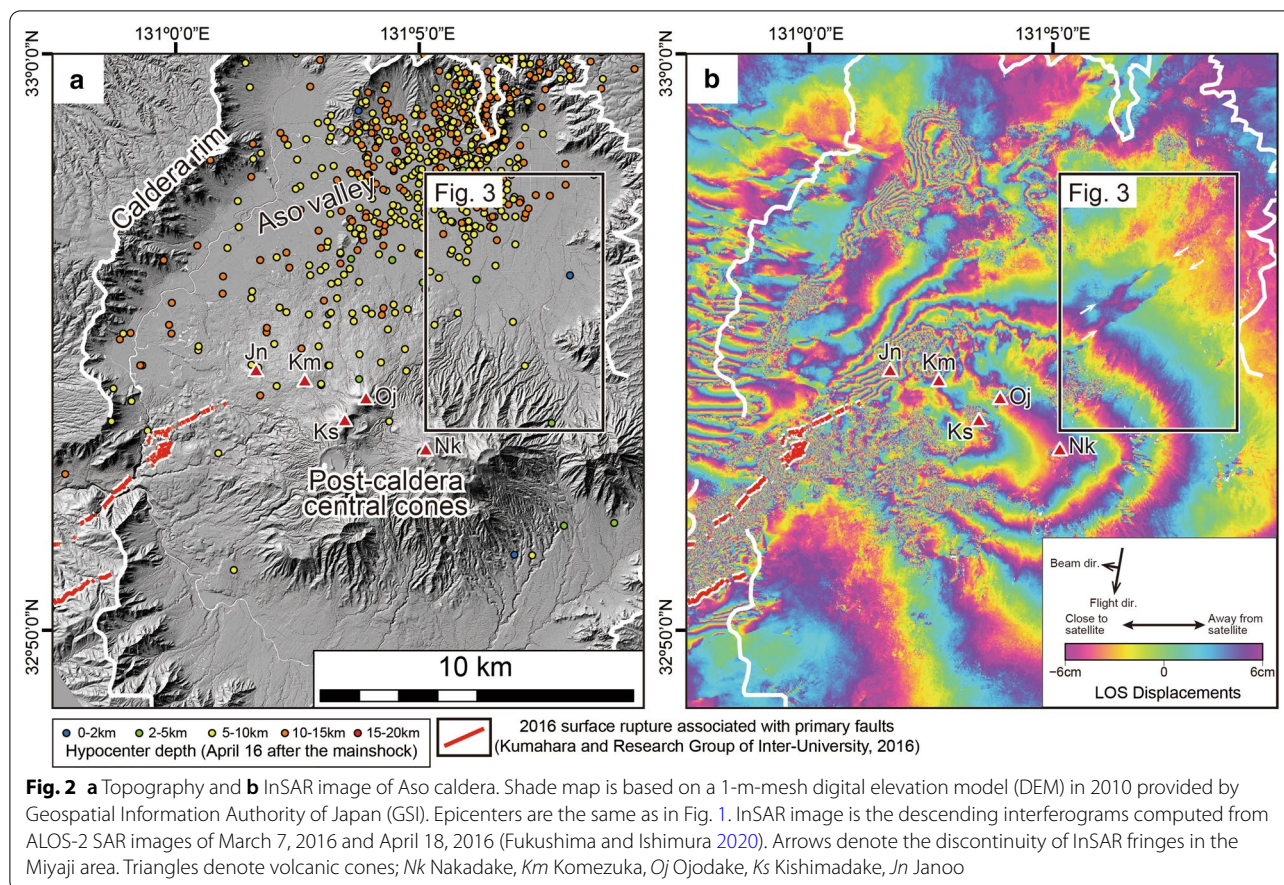
### Geological setting

Central Kyushu is structurally characterized by the Beppu–Shimabara graben (Fig. 1; Matsumoto 1979), where a north–south extension has been ongoing since 6 Ma (Kamata and Kodama 1994). In this graben, there are many east–west striking normal faults (Research Group for Active Faults of Japan 1991) and volcanic activity. The study area, the Aso caldera, is located in the central part of the Beppu–Shimabara graben. The caldera was formed by the recent caldera-forming eruptions from 300 to 90 ka (Ono and Watanabe 1985; Aoki 2008) (Figs. 1 and 2). Eruption episodes and tephra sequences deposited since the latest caldera-forming event (Aso-4) (87 ka; Aoki 2008) were determined by Miyabuchi (2009),

providing accurate age constraints for paleoseismic studies. Volcanic activity during the last 15 ka was identified by soil and tephra alternations and was divided into 16 periods (N1–N16) from youngest to oldest (Fig. 3a; Miyabuchi and Watanabe 1997). According to Miyabuchi (2009), major tephra during the last 10 kyr were erupted from the post-caldera central cones (Fig. 2): Aso central cone pumice 1 (ACP1) (4.1 ka), Kishimadake scoria (KsS) (4 ka), Ojodake scoria (OjS) (3.6 ka), and Nakadake N2 scoria (N2S) (1.5 ka).

The Futagawa fault is a 20-km-long dextral strike-slip fault (Nakata and Imaizumi 2002). Prior to the 2016 event, vertical and horizontal slip rates were estimated to be 0.1–0.3 mm/yr and 0.2 mm/yr, respectively, and at least, two faulting events have been identified since 28 ka based on trench studies (Headquarters for Earthquake Research and Promotion 2013). However, after the 2016 event, the vertical and horizontal slip-rate estimates were corrected to be 0.9–1.1 mm/yr and 1.5–3.7 mm/yr, respectively, a one-order of magnitude higher than





those estimated before the 2016 event (Ishimura 2019). Moreover, multiple events since Kikai-Akahoya (K-Ah) tephra (7.3 ka; Smith et al. 2013) were identified by many paleoseismic trench excavations (e.g., Tsutsumi et al. 2018; Okamura et al. 2018; Toda et al. 2019). Additionally, the Futagawa fault was extended to the inside of the caldera based on a reexamination of tectonic geomorphology after the 2016 event (Kumahara et al. 2017a, b; Suzuki et al. 2017). The tectonic geomorphological and paleoseismological studies after the 2016 event revealed that the Futagawa fault is more active than previously estimated.

The Futagawa fault generated the April 16 mainshock (Mw 7.0) of the 2016 Kumamoto earthquake sequence, and the primary surface ruptures appeared along the previously mapped active fault traces (Fig. 1; Kumahara and Research Group of Inter-University 2016; Shirahama et al. 2016; Okamura et al. 2018). The surface ruptures extending northeast cut the caldera rim and also appeared inside of the caldera (Figs. 1 and 2). The maximum dextral displacement was approximately 2–3 m observed in the central part of the Futagawa fault and approximately 0.5–1.0 m in the caldera (Shirahama et al. 2016; Okamura et al. 2018). In

the western half of the rupture zone, differential lidar analysis revealed a 3D deformation of the 2016 event (Moya et al. 2017; Scott et al. 2018), whose results were consistent with the field observations. Many secondary surface ruptures appeared on the mapped and unmapped active fault traces (Fujiwara et al. 2016). Mass movement on the slopes and lateral movements also occurred in the caldera (Tsuiji et al. 2016; Fujiwara et al. 2017; Tajima et al. 2017; Saito et al. 2018).

Our research site in the Miyaji area is on an alluvial fan surface in the northeast foot of the post-caldera central cones in the caldera (Fig. 2). The site is 10 km away from the eastern edge of the primary surface rupture, and neither a mass movement nor a lateral movement occurred near the site. Around the Miyaji area, field observations confirmed discontinuities in InSAR fringes (Fig. 2) with small surface ruptures (Ishimura et al. 2017).

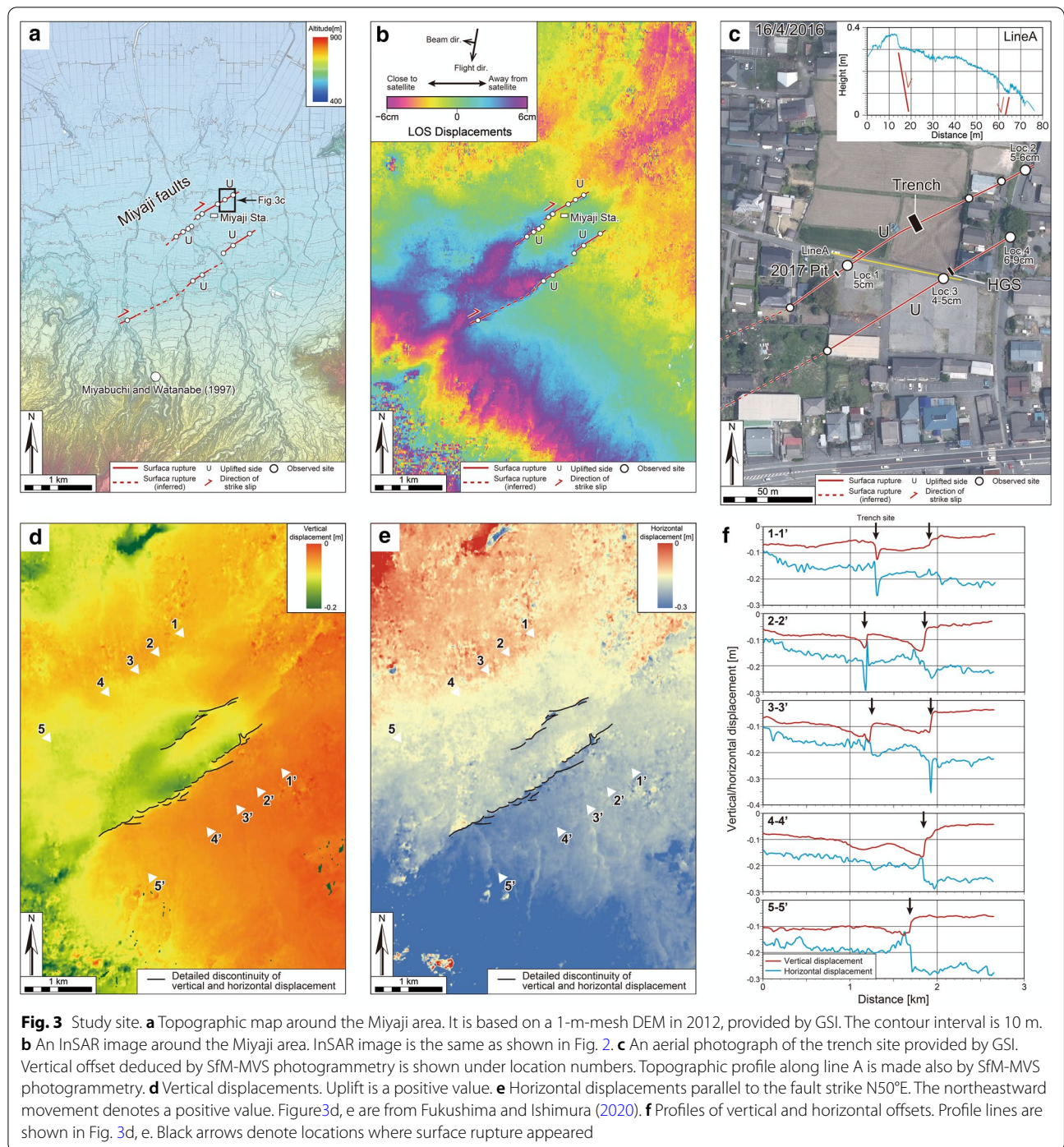
## Methods

### Field survey

#### Field mapping

In May 2016, we conducted a preliminary field survey to check surface ruptures along discontinuities that





appeared in the InSAR fringes reported by the Geospatial Information Authority of Japan (GSI). At the time, surface ruptures were mapped and displacements were measured (Ishimura et al. 2017). In 2017, we mapped the surface ruptures around the trench in detail before the trench excavation. For measuring the amount of

vertical displacements of the surface ruptures, we used the Structure-from-Motion and Multi-View Stereo (SfM-MVS) photogrammetry software (Agisoft PhotoScan, professional version). In addition, we interviewed inhabitants about the timing of the appearance of surface ruptures in the Miyaji area.

### Paleoseismic surveys

In October 2017, we excavated a trench in a paddy field that was 9 m long, 5 m wide, and 3 m deep. We then established a grid system on a 60°–70° slope and logged the trench walls. For tephra analysis and radiocarbon dating, we took samples from the walls. Moreover, we excavated a pit with a depth of 0.7 m on the trench floor.

Another surface rupture trace was estimated to be in the corner of the rice paddy field where the trench was excavated. Since the excavation area was limited, we conducted a coring survey there. For coring, we used Handy Geoslicer (hereinafter, HGS; Nakata and Shimazaki 1997; Takada et al. 2002) and obtained eight HGS cores. A total station was used to measure the locations of the trench and coring sites.

### Laboratory work

#### Tephra analysis

Samples of tephra were washed using a 62- $\mu\text{m}$  nylon mesh and dry sieved using a 120- $\mu\text{m}$  nylon mesh. The refractive index of volcanic glass shards was measured with a refractive index measuring system (RIMS 2000; Kyoto Fission Track Co., Ltd.) using the 62–120  $\mu\text{m}$  fractions. The RIMS system measures the refractive index of volcanic glass shards with an accuracy of  $\pm 0.0002$  (Danbara et al. 1992).

#### Radiocarbon dating

Radiocarbon dating was conducted for eight samples using an accelerator mass spectrometer in the Institute of Accelerator Analysis Ltd. The obtained age data were calibrated on the basis of the IntCal13 calibration curve (Reimer et al. 2013) using the OxCal 4.3 program (Bronk Ramsey 2009) (Table 1). Bayesian analysis in the OxCal program (Bronk Ramsey 2008) was used to calculate the age of the penultimate event and tephra.

## Results

### Observation of the surface ruptures and displacements around the trench site

In the Miyaji area, there were two northeast–southwest striking faults (hereinafter, north and south faults) in the discontinuities of InSAR fringes (Figs. 2b, 3a, b, and 4; Ishimura et al. 2017), which we called the Miyaji faults. The Miyaji faults exhibited a dextral slip, which was consistent with the InSAR measurements (Fig. 3d–f; Fukushima and Ishimura 2020). These surface ruptures appeared on the alluvial fan surface at the foot of the Aso volcano where no traces of active faults were previously mapped. Even after the 2016 event, based on aerial photographs and high-resolution digital elevation models (DEMs), it was not possible to identify tectonic geomorphic features indicative of active faulting.

Damage was observed on the surface of paved roads and concrete walls (maximum vertical separation: 10 cm, maximum dextral slip: 5 cm) (Figs. 3 and 4; Ishimura et al. 2017). Fukushima and Ishimura (2020) created 3D deformation maps using InSAR data observed from three different directions and GNSS data (Fig. 3d, e). From these detailed vertical and fault-parallel horizontal displacement fields, it was found that the lengths of the north and south faults were approximately 1.5 km and 3.2 km, respectively. The maximum vertical and dextral displacements were 8 cm up on the south and 19 cm for the north fault, and 12 cm up on the south and 19 cm for the south fault. In addition, the vertical and fault-parallel horizontal displacement fields (Fig. 3d, e) showed left-stepping en-echelon surface ruptures in both faults. The geometry of these faults was consistent with the dextral slips on the faults. Local subsidence occurred at the trench site, forming a small graben (Fig. 3d).

At the trench site, two surface ruptures were found forming a small graben (Fig. 3c). We confirmed that the

**Table 1** Radiocarbon dates of samples from the trench

Sample No	Labo No	Sample position (unit No.)	Grid No	Depth from 0 m grid [m]	Material	$\delta^{13}\text{C}$ [‰]	Conventional $^{14}\text{C}$ age [yrBP]	Calibrated age ( $2\sigma$ ) [calBP]
1	IAAA-171171	10	W4.15	0.24	Organic sediments	$-11.43 \pm 0.48$	$1,180 \pm 20$	1180–1050 (95.4%)
2	IAAA-171170	Top of 40	W5.65	0.57	Organic sediments	$-13.64 \pm 0.38$	$1,900 \pm 20$	1900–1810 (95.2%), 1760–1740 (0.2%)
3	IAAA-171454	Bottom of 40	W5.65	0.86	Organic sediments	$-12.29 \pm 0.39$	$2,070 \pm 20$	2120–1990 (95.4%)
4	IAAA-171453	Top of 60	W5.65	1.04	Organic sediments	$-13.83 \pm 0.45$	$2,620 \pm 30$	2780–2720 (95.4%)
5	IAAA-171169	Bottom of 60	W5.65	1.18	Organic sediments	$-9.50 \pm 0.30$	$2,640 \pm 20$	2780–2740 (95.4%)
6	IAAA-171172	80	E8.05–8.10	1.85–1.90	Charcoals	$-12.00 \pm 0.47$	$2,990 \pm 20$	3230–3070 (95.4%)
7	IAAA-171509	80	E7.98	1.83	Organic sediments	$-12.69 \pm 0.34$	$3,010 \pm 20$	3330–3300 (5.9%), 3260–3140 (88.0%), 3100–3080 (1.5%)
8	IAAA-151561	Bottom of 101	N3.9	2.27	Charcoals	$-24.47 \pm 0.33$	$3,070 \pm 20$	3360–3220 (95.4%)



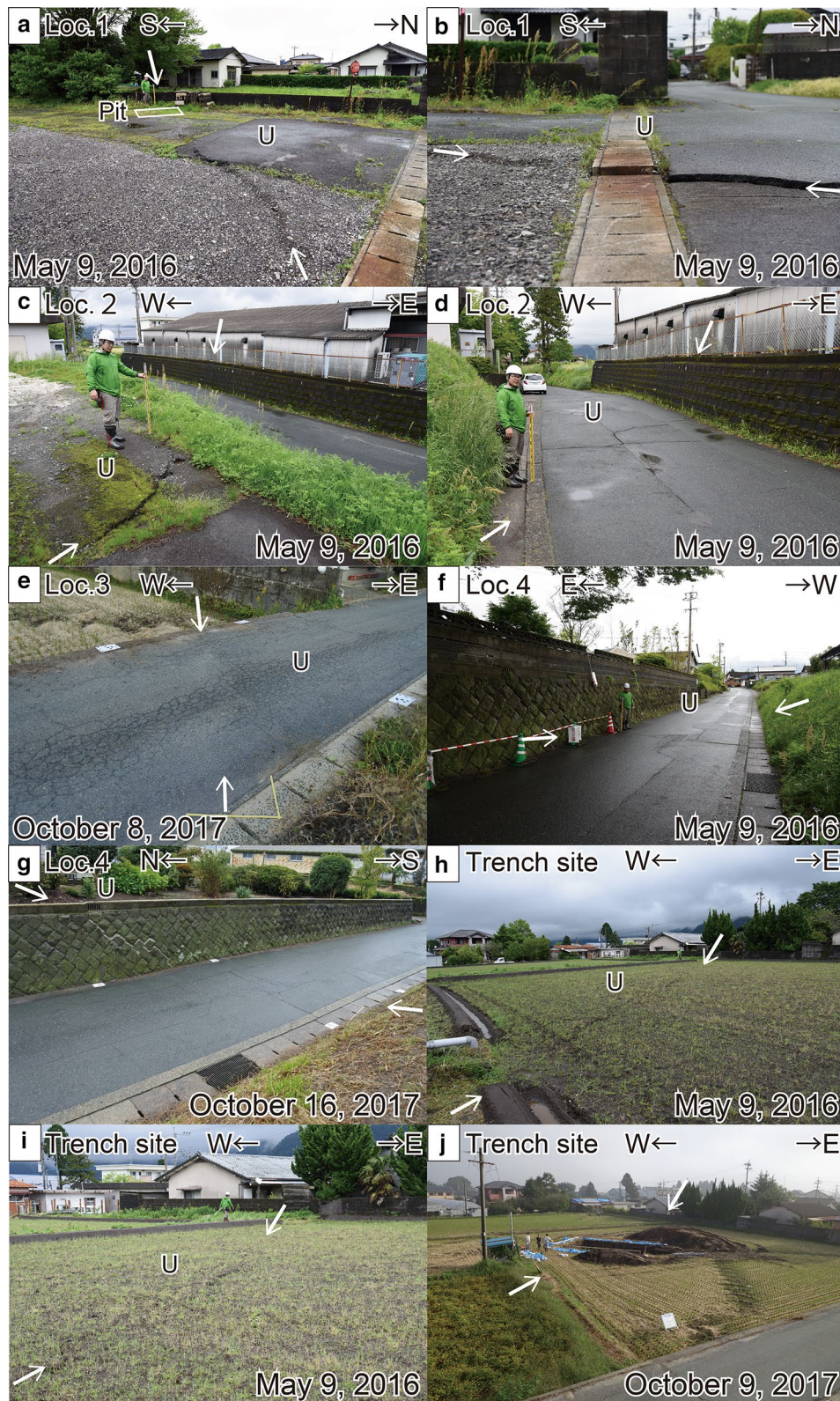


**Fig. 4** Photographs of surface ruptures around the trench site. Location numbers are shown in Fig. 3c. Arrows denote the surface ruptures. U: uplifted side. Photos of C and H are modified after Ishimura et al. (2017)

northern trace was associated with a dextral and vertical (northwest up) slip, and that the southern trace was associated with a vertical (southeast up) slip. Digital surface models were built to measure the surface displacements on paved roads based on SfM-MVS photogrammetry. Both surface ruptures showed approximately 5 cm of vertical displacement (Fig. 3c, Line A), which was consistent with the InSAR measurements (Fig. 3f, Line 1–1').

Two inhabitants, living on the north and south faults, mentioned that the small surface ruptures appeared during the mainshock of the 2016 Kumamoto earthquake sequence, not at the foreshock and aftershocks. From this information, it was confirmed that the surface ruptures in the Miyaji area were associated with the mainshock of the 2016 Kumamoto earthquake.

### Paleoseismic surveys across the small graben

#### Trench survey

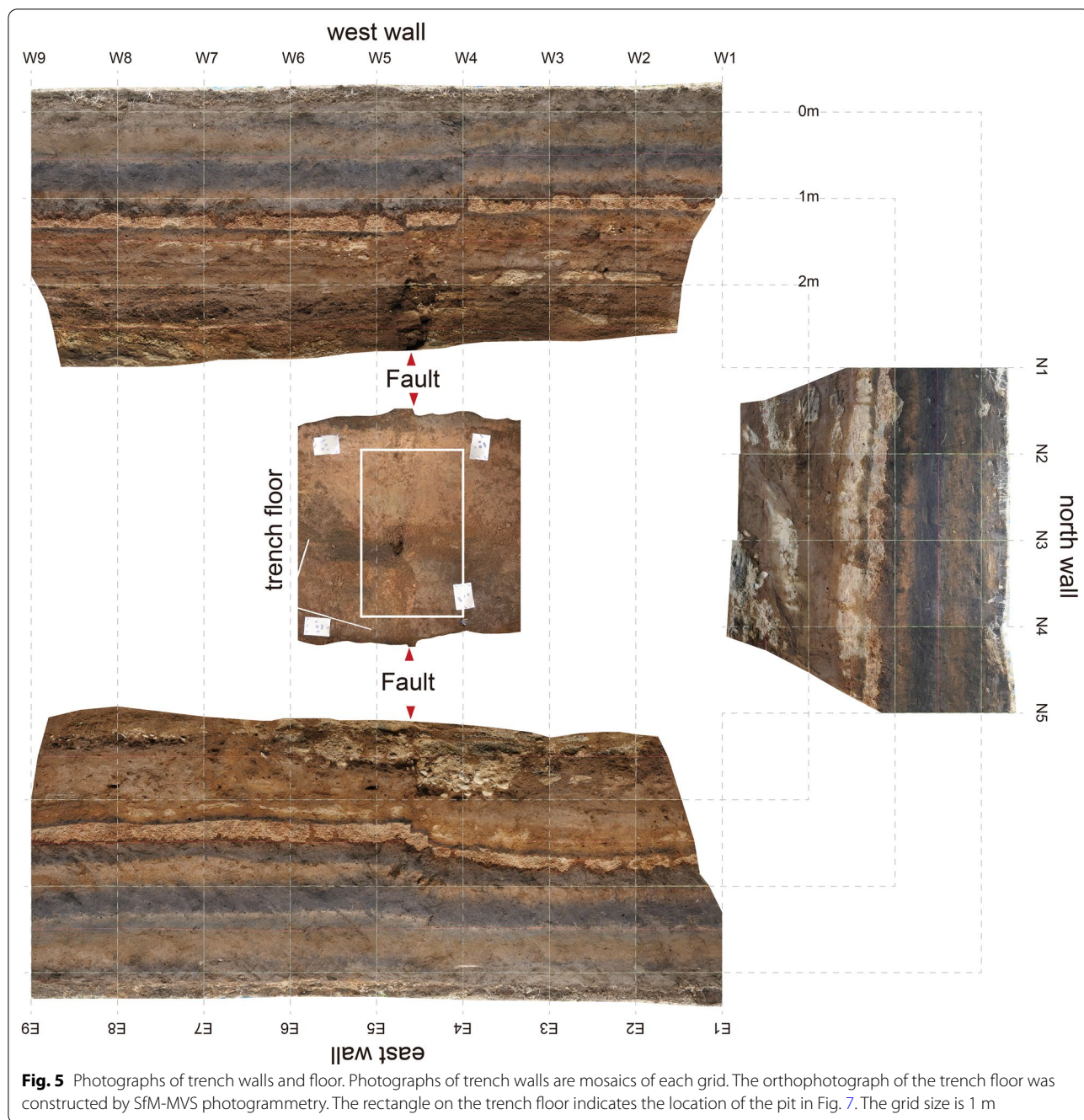
The deposits in the trench walls were divided into 20 units (unit 00–111) based on composition, facies, and structure. Figures 5 and 6 show views of the trench and logs in the three walls and trench floor, and provide a brief description of the stratigraphic units. Table 1 shows the radiocarbon dates.

Units 00 and 01 were the cultivated soil and sediments of the post- and pre-2016 events, respectively. Units 10–80 were soil and tephra sequences, which were mostly aeolian deposits. The basement of unit 20 is a little erosive and units 30 and 31 were partially laminated. However, clear channels and large erosion features were not found. Therefore, it was interpreted that the soil and tephra sequences were continuously deposited during the formation of units 10–80. Units 90–111 were fluvial sediments, but unusual sedimentary structures and stratigraphy were recognized between units 101 and 110 on the northern wall and trench floor. Units 103 and 110 had almost similar compositions (black scoria) and sedimentary structures and unit 101 was distributed above units 103 and 110 on the western and eastern walls, however, on the northern wall, the lower part of unit 101 was interbedded between units 103 and 110. Moreover, on the northern wall, unit 101 partially intruded to unit 103, and the lower western part of unit 101 showed shear structures, indicating a fluidized deformation in unit 101. The boundary between units 101 and 110 was also traceable from the northern wall to the trench floor, and its strike was parallel to the topographic slope and was perpendicular to the faults (Fig. 6). The sedimentary structures and the direction of basal contacts of unit 101 suggest that the mobile blocks mainly composed of unit 103 on the western and northern walls were associated with liquefaction and lateral movement, and probably moved from south to north following the topographic slope.

To confirm the slip surface of the mobile blocks, a pit was excavated to a depth of 0.7 m from the trench floor across the faults (Figs. 5 and 6), and a basal gravel layer was further 35 cm below the trench floor on the uplifted side. The basal gravel layer contained horizontally bedded pebble- to cobble-sized rounded gravels (Fig. 7). On the other hand, unit 110 was deformed and thinned to the west, showing a wedge-like geometry. A slip surface was recognized inside or in the base of unit 110 (Fig. 7). From this observation, we interpreted that the mobile block slid over the gravel layer, deforming units 101, 110, and 111 on the northern wall and trench floor. In addition, unit 102 was distributed in a patchy texture on the northern and eastern walls, and their gravels were identical to the basal gravel layers in the pit (Fig. 7). Therefore, unit 102 was probably transported by liquefaction and/or involved in the lateral movement.

Tephra and radiocarbon dating were used to estimate the age of each unit. Five types of tephra were identified based on petrographic characteristics, sedimentary facies, stratigraphy, and radiocarbon ages. Unit 30 consisted of brown to green volcanic glasses whose stratigraphy and sedimentary facies are similar to those observed in the 2017 pit near our trench site (Fig. 3c; Ishimura et al. 2017). Ishimura et al. (2017) identified deposits similar to unit 30 as the N2S tephra (Miyabuchi and Watanabe 1997; Miyabuchi 2009) erupted from Nakadake volcano (Fig. 2) based on the refractive indices of volcanic glass shards. The age of N2S tephra is estimated to be 1490–1470 cal BP (68.2%) (Yamada et al. 2017) based on a high-precision age model of marine core sediments in the Beppu Bay. The radiocarbon ages below and above unit 30 are consistent with the tephra age, confirming that unit 30 is correlated with the N2S tephra. Units 50 and 51 consisted of orange scoria and volcanic ash, and radiocarbon ages above and below them are  $2070 \pm 20$  yr BP and  $2620 \pm 30$  yr BP, respectively. Based on the stratigraphy and radiocarbon ages in Miyabuchi and Watanabe (1997), these units correspond to the N3 volcanic activity period. Unit 70 was a characteristic layer composed of reddish scoria. Radiocarbon ages obtained above and below this unit are  $2640 \pm 20$  yr BP and  $3010 \pm 20$ ,  $2990 \pm 20$  yr BP, respectively. Based on stratigraphy, sedimentary facies, and radiocarbon ages, unit 70 is correlated with the OjS tephra that was erupted from Ojodake volcano (Fig. 2). Although its age was estimated to be 3.6 ka (Miyabuchi, 2009), the age of OjS tephra is updated to be 3180–2790 cal BP (95.4%) based on Bayesian analysis using the OxCal program (Additional file 1: Fig. S2). Units 103 and 110 were scoria-dominated fluvial sediments, characteristically containing black scoria. The radiocarbon age obtained from unit 101 is  $3070 \pm 20$  yr BP. Based on stratigraphy, sedimentary facies, and radiocarbon age, units





103 and 110 are correlated with the KsS tephra (4.0 ka; Miyabuchi 2009) that was erupted from Kishimadake volcano (Fig. 2). Unit 111 contained sparse white pumice (diameter: less than 1 cm). The refractive indices of volcanic glass shards of this white pumice ranged from 1.505 to 1.508 (Mode:1.505), which are similar to those of ACP1 tephra (4.1 ka; Miyabuchi 2009) reported by Furu-sawa and Umeda (2000). From the standpoint of refractive index and stratigraphy, the white pumice included

in unit 111 is correlated with the ACP1 tephra that was erupted from Janoo volcano (Fig. 2) (Miyabuchi 2017). However, ACP1 horizon could not be clearly identified in unit 111, so we infer that unit 111 is at the same age as ACP1 or younger.

We recognized several faults cutting up to unit 01 on both walls (Figs. 5 and 6). Two faults were recognized mainly on the western wall. The northern fault cut unit 01, and two branches were identified in unit 101. The

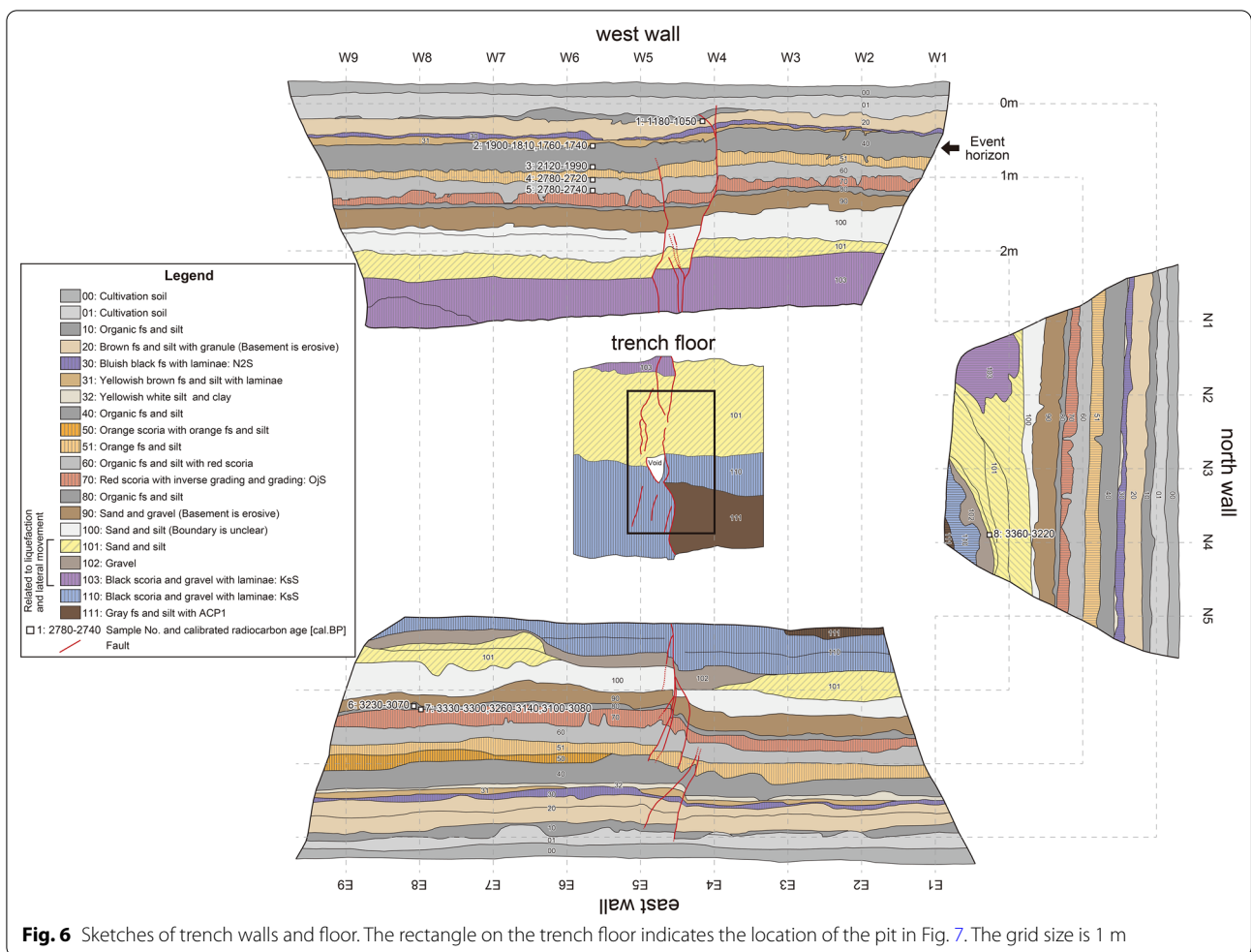


**Fig. 6** Sketches of trench walls and floor. The rectangle on the trench floor indicates the location of the pit in Fig. 7. The grid size is 1 m

southern fault displaced the bottom of unit 40. In the eastern wall, two groups of faults were recognized. One group consisted of two faults above unit 60 and the other consisted of multiple faults between units 110 and 40. The former displaced the bottom of unit 01, and the latter cut into unit 40. These faults represented a typical flower structure, suggesting strike-slip displacement. The vertical offset of each layer is shown in Fig. 8. This shows the difference in vertical offset above and below unit 40. The vertical offset above unit 40 was about 10–15 cm and that below unit 40 was about 20–35 cm, which was twice the latest event. In addition, the vertical offset of the basal gravel layer was 25–30 cm on the eastern wall of the pit at the trench floor.

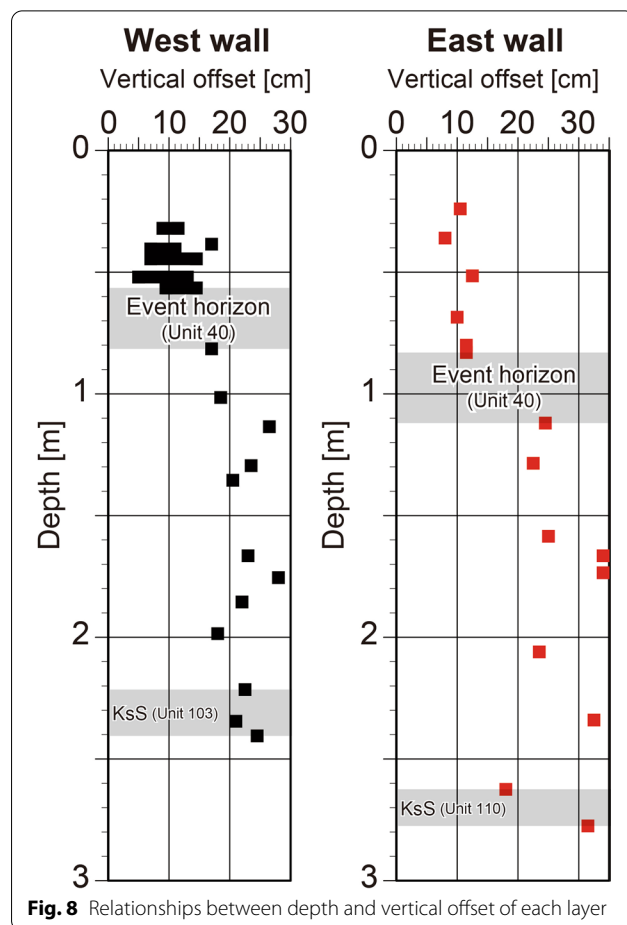
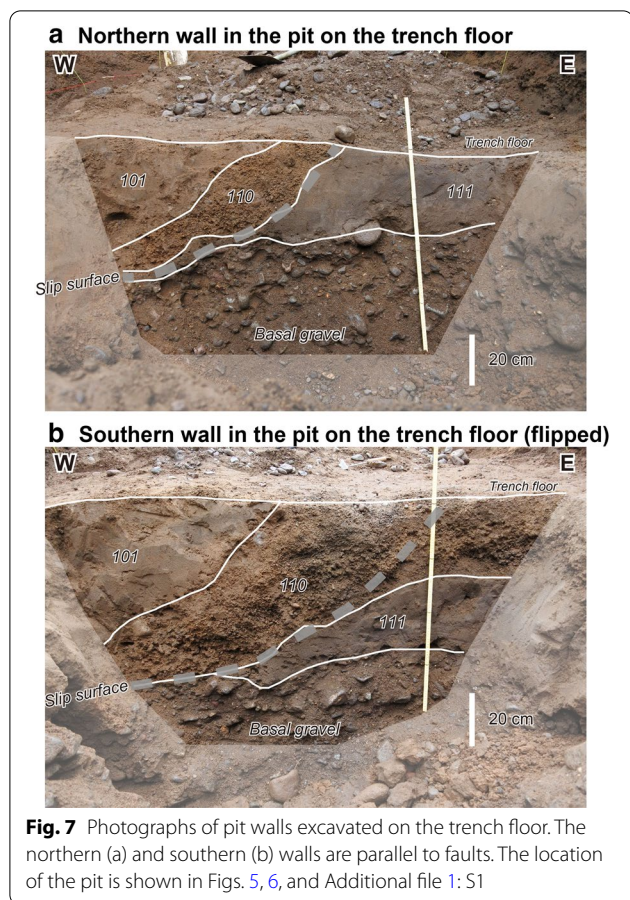
**Handy Geoslicer survey**

The HGS cores were obtained from the southeastern corner of the rice paddy field (Fig. 3c), about 30 m southeast of the trench. The same unit labels were used for the deposits in the HGS cores (Fig. 9). Although the

HGS core deposits were roughly correlated with the trench deposits, units 20–32 were absent from the HGS coring site, probably due to the artificial modification of the rice paddy field. Units 02 and 03, which were not identified in the trench, were also related to artificial modification and cultivation.

In HGS6, a fault that cut up to unit 01 was identified, indicating that this faulting was associated with the 2016 event (Fig. 9). Based on the height difference between the layers of HGS5 and HGS6, a fault with a branch recognized in HGS6 was estimated between the cores. The vertical separation between units 03–90 was about 10 cm. Therefore, this fault moved only during the 2016 event since the deposition of unit 90. On the other hand, between the HGS2 and HGS3, a height difference was found between units 51 and 90, but the height difference was not identified in unit 01, indicating the occurrence of an event older than the 2016 event.





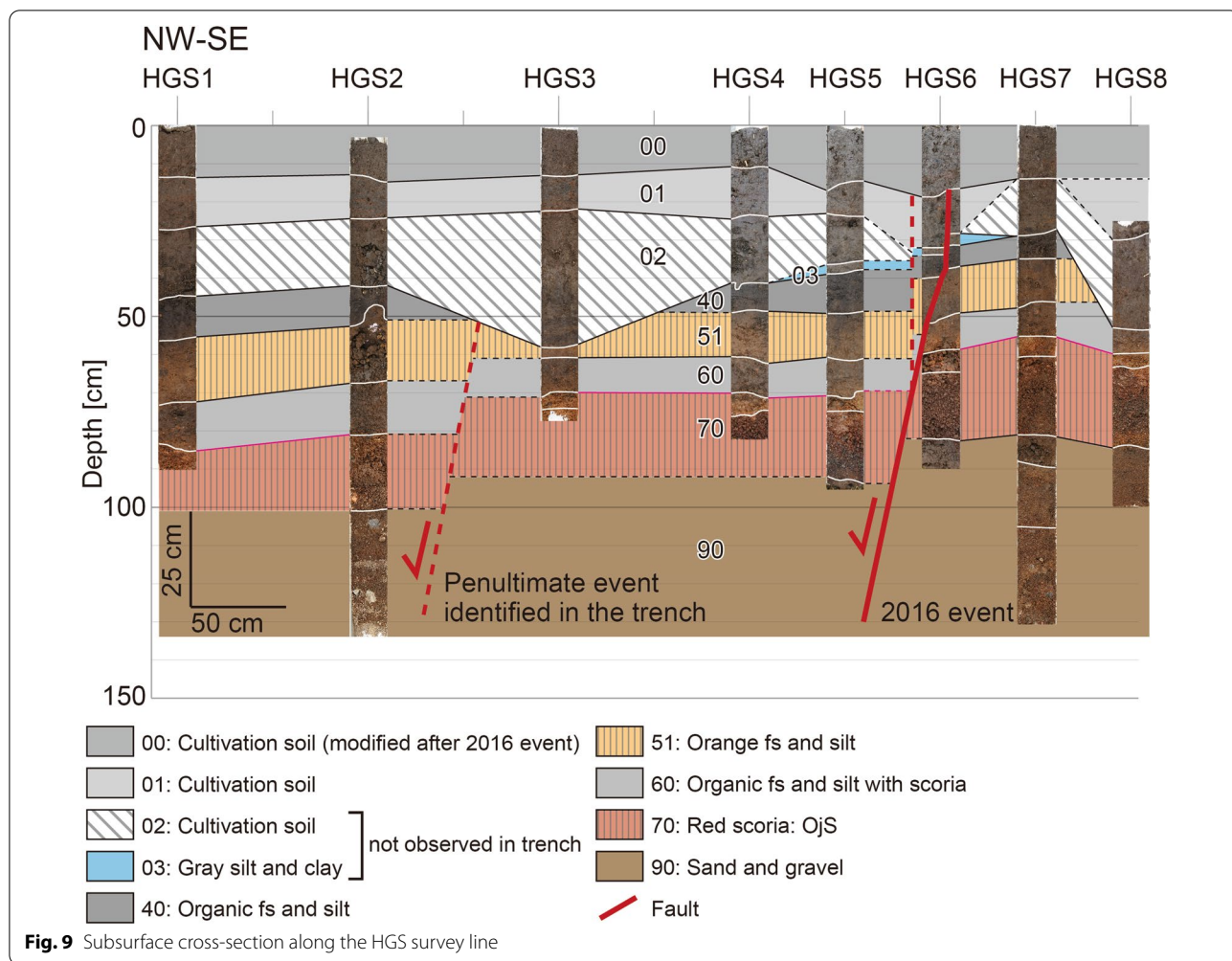
**Discussion**

**Paleoseismic events on research site**

The lower part of unit 40 in the trench was displaced by the branch faults; however, the upper part was not displaced and was covered by units 31 and 32. This indicates that the penultimate event occurred during the deposition of unit 40. The depth profile of the vertical offset of each layer (Fig. 8) also supports this interpretation. Evidence of the 2016 event and an older event corresponding to the trench results were also found in the HGS cores. The age of unit 40 was constrained by tephra layers and radiocarbon ages. Based on Bayesian analysis using the OxCal program, the age of the penultimate event was estimated to be 2080–1830 cal BP (95.4%) (Additional file 1: Fig. S2).

A candidate for the antepenultimate event was the event resulting in liquefaction and lateral movement identified in unit 101, which was probably caused by strong ground motions. As for the timing of this event, if liquefaction and lateral movement occurred underground at the faulting events in AD2016 and/or 2080–1830 cal BP, some broad deformations should be identified in the overlying sediments and on the ground

surface. However, such deformation was identified neither in sediments above unit 90 nor ground surface, thereby implying that the timing of liquefaction and lateral movement was at least before unit 90 deposition. Furthermore, the vertical offset of the faults (Fig. 8) indicates that there were only two faulting activities after the deposition of the KsS tephra. These details suggest that this liquefaction and lateral movement were not related to the faulting events of the Miyaji faults. Thus, we interpret that the disturbed features of unit 101 are attributed to strong ground motions due to volcanic activity. From tephrostratigraphy, this event occurred between OjS and KsS tephras erupted from Ojodake and Kishimadake volcanoes (Fig. 2). OjS and KsS tephras are the major sub-plinian basaltic scoria fall deposits including three fall units during the Holocene (Miyabuchi 2009), which led to the formation of scoria cones. Furthermore, Miyabuchi and Watanabe (1997) introduced at least two scoria fall units between OjS and KsS tephras, suggesting that other sub-plinian eruptions occurred during that period. Therefore, the strong ground motions associated with these eruptions



probably resulted in the liquefaction and lateral movement recognized in unit 101.

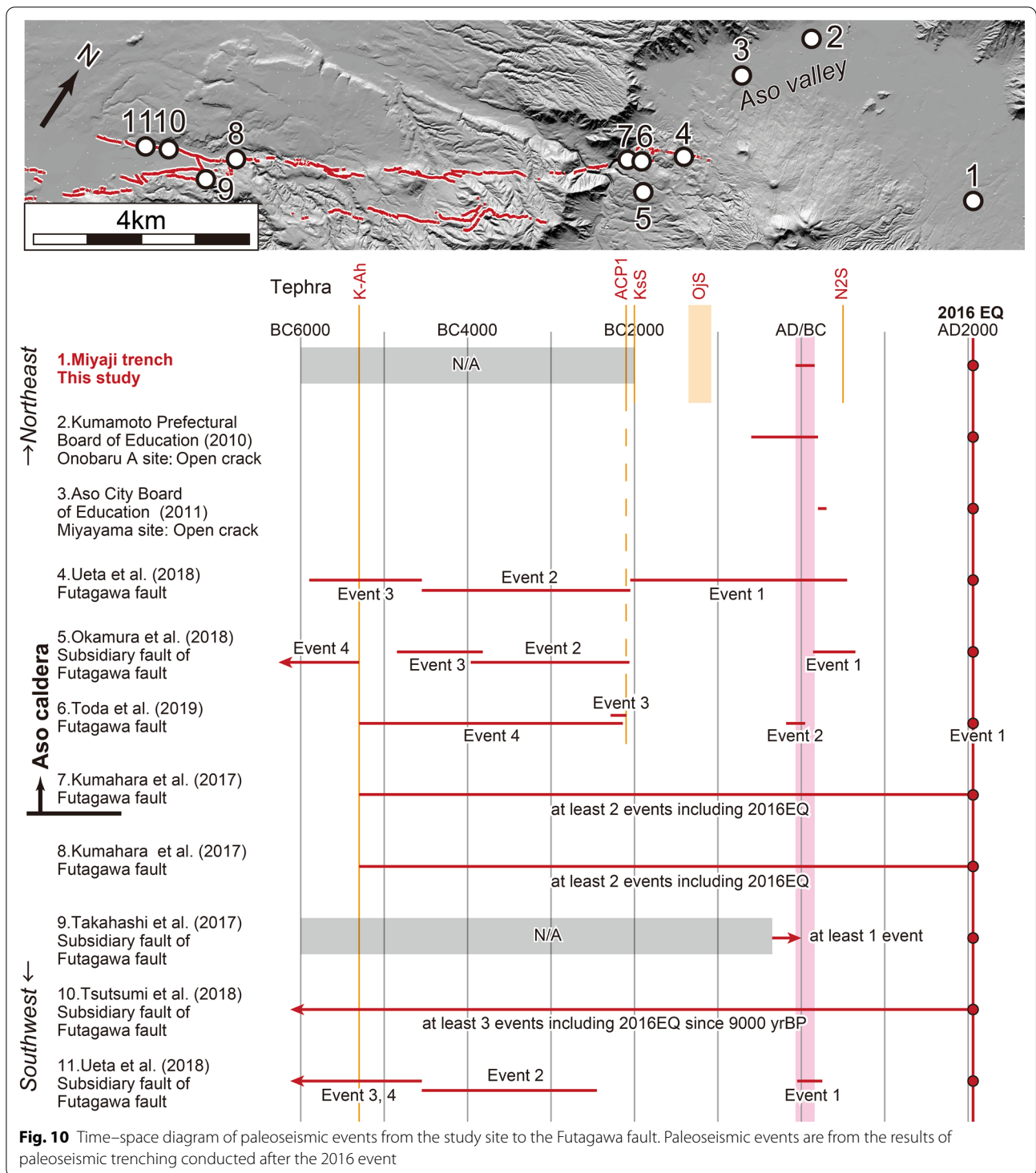
Two paleo-faulting events, including AD2016 and 2080–1830 cal BP, were found in the Miyaji trench since the KsS tephra (4.0 ka), and the inter-event times between the two events is 1896–2146 years. Using this interval and the displacement found from the InSAR analysis of the 2016 event, we simply calculated the slip rates for the Miyaji faults. The vertical and horizontal slip rates of the north fault were 0.04 mm/yr and 0.09–0.10 mm/yr, respectively. Those of the south fault were 0.06 mm/yr and 0.13–0.14 mm/yr, respectively. These values are classified into the lowest class of the active fault slip rates that can be detected based on tectonic geomorphology in Japan (e.g., Research Group for Active Faults of Japan 1991).

**Comparison with paleoseismic events at other sites**

Figure 10 shows the results of paleoseismic studies at other sites. In the Aso caldera, open cracks showing

lateral spreading were observed at two archeological sites. At the Onobaru archeological site, the event age was estimated to be 2600–1800 years ago based on radiocarbon dating and pottery chronology (Kumamoto Prefectural Board of Education 2010). At the Miyayama archeological site, the event age was estimated to be around the third century based on archeological remains (Aso City Board of Education 2011). In the 2016 event, open cracks, lateral spreading, and liquefaction were observed extensively along the Aso valley (Fig. 2; Tsuji et al. 2016; Fujiwara et al. 2017). Considering these phenomena observed in the 2016 event, the open cracks found at the archeological sites indicated that deformations similar to the 2016 event occurred in the past. In the paleoseismic studies of the Futagawa fault after the 2016 event, multiple events were identified since the K-Ah tephra (7.3 ka). Moreover, some of these studies suggested that the ages of the penultimate event of the Futagawa fault in the Aso caldera were approximately 2 ka (Ueta et al. 2018;





Toda et al. 2019). The correspondence of the penultimate event age between the Miyaji area and other sites indicates that surface deformations similar to the 2016 event occurred in ca. 2 ka at each site. In addition, our

age constraints for the penultimate event were more robust and accurate than other paleoseismic study sites, because the event horizon was identified using tephra and soil layers and vertical offsets, and well-known tephtras were found above and below the event horizon.

### Behavior of the Miyaji faults

Based on the inversion modeling of InSAR analysis, the north and south faults in Miyaji dip 63° and 42° to the northwest, and the slips are limited to areas shallower than 1.5 km deep (Fukushima and Ishimura 2020). From these fault models and slip distributions, the Miyaji faults are inferred to be the faults separated from the subsurface seismogenic fault extended from the primary fault in the western Aso caldera. Besides, the following information suggests that the Miyaji faults have been triggered at least in the recent two events by the primary fault (Futagawa fault) activity: 1) surface ruptures in the Miyaji area occurred simultaneously with the activity of the primary fault in 2016, 2) the amount of vertical offset due to the 2016 event is almost the same as that of the penultimate event in the trench, and 3) the penultimate event age of the north fault in the Miyaji area corresponds to that of the primary fault. Considering the extremely shallow slip depth of the Miyaji faults and the features of the faults mentioned above, we presume that they are unable to generate large earthquakes. The epicenters and depths of aftershocks (Figs. 1 and 2) of the 2016 Kumamoto earthquake sequence around the Miyaji area support this interpretation. This characteristic is completely consistent with a fully aseismic type of low-slip-rate active faults (Toda and Ishimura, 2019; Fig. 11c). This type means that the fault is not a source fault, but the fault slips are always triggered by large earthquakes generated by the adjacent major active faults.

Other secondary surface ruptures in the northwest of the Aso caldera identified by InSAR (Fig. 2; Fujiwara et al. 2016) are similar to the Miyaji faults in terms of fault length, slip rate, and their characteristics during the 2016 event. A paleoseismic trench across one of the triggered faults indicated three surface cutting events, including the 2016 event since 3500 cal BP (Une et al. 2019). It is confirmed that the fault has moved more frequently than expected by the slip rate (0.1 mm/yr; Research Group for Active Faults of Japan 1991). Therefore, we hypothesize that the secondary faults on the northwestern caldera rim reported by Fujiwara et al. (2016) behave similarly to those found around the Miyaji area.

On the other hand, the paleoseismicity of LSRAF in Fukushima and Ibaraki prefectures revealed that the activities of LSRAFs were not always triggered by the past megathrust earthquakes along the Japan Trench (Toda and Tsutsumi 2013; Miyashita 2018; Komura et al. 2019). In these cases, LSRAFs moved from a week to a month after the 2011 event, causing large earthquakes themselves. This behavior of the LSRAFs is quite different from that of the Miyaji faults. Therefore, LSRAFs in Fukushima and Ibaraki cases could be either completely seismogenic or variable types (Fig. 11a, b). These

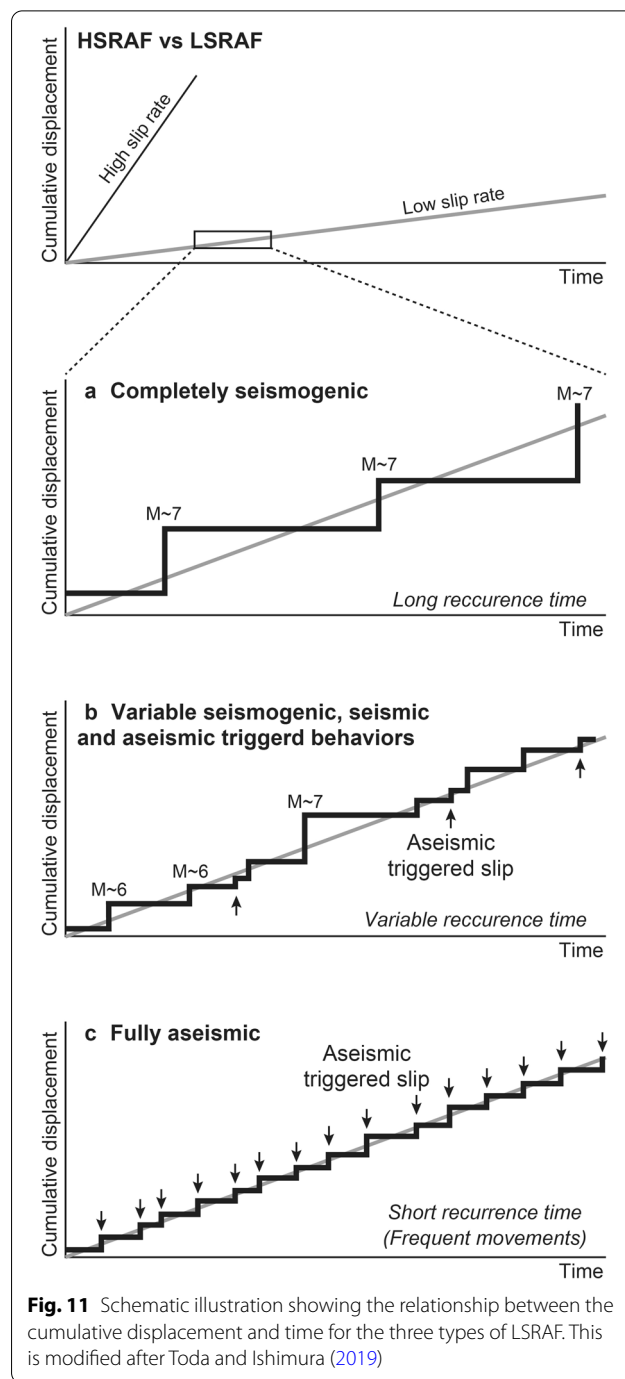


**Fig. 11** Schematic illustration showing the relationship between the cumulative displacement and time for the three types of LSRAF. This is modified after Toda and Ishimura (2019)

different behaviors of LSRAFs represent the difficulty of the understanding of LSRAFs and their risk assessment of seismic and displacement hazards. Therefore, in addition to finding small surface ruptures detected by recent space geodesy, the behavior of LSRAFs needs to be reviewed by obtaining paleo-slip evidence of them. This is also important for the grouping of active faults,



establishing active fault activity scenarios, and assessing risks of fault displacement.

#### Development of tectonic geomorphology by small but frequent slips

Even if an active fault is short and its slip rate is low, the fault topography (e.g., fault scarp) is generally considered to be formed by large earthquakes, which can displace the ground surface. This assumption applies to a completely seismogenic type for a low-slip-rate active fault (Fig. 11a). However, recent geodetic observations and this study suggested that some of the minor active faults were probably developed by large earthquakes on the adjacent major faults. In the 2016 Kumamoto case, a vertical offset of less than a few decimeters occurred on broadly and remotely distributed surface ruptures around the primary fault (Fujiwara et al. 2016; Toda et al. 2016; Goto et al. 2017). If such small slips have occurred frequently on LSRAFs associated with large earthquakes by the adjacent HSRAFs, the total offset accumulated by small but frequent slips may be sufficient to explain the present fault topography (e.g., active faults in the northwest of the Aso caldera). In this case, the subtle fault topography associated with LSRAFs does not necessarily indicate the presence of subsurface seismogenic faults. To examine such fault topography development associated with LSRAFs and/or secondary faults, we need to study the timing and displacement of paleo-slip on them. Moreover, our results suggest that the timing of paleo-slip on secondary faults may indicate the timing of nearby primary fault paleoseismic events.

#### Conclusions

We conducted a field mapping of small surface ruptures associated with the 2016 Kumamoto earthquake sequence, and a paleoseismic trenching in the Aso caldera. Field mapping revealed that small but clear surface ruptures on the InSAR fringe discontinuity were associated with the mainshock, not the foreshock and aftershocks of the 2016 event. InSAR-derived 3D deformation data were consistent with the field measurement, confirming that the north and south surface ruptures around the Miyaji area were dextral south-up active faults with lengths of approximately 1.5 km and 3.2 km, respectively. Paleoseismic trenching revealed that the penultimate event occurred at ca. 2 ka with the same amount of vertical offset at the 2016 event. The penultimate event of the Miyaji faults corresponds to that of the primary fault (Futagawa fault), indicating that the Miyaji faults also moved simultaneously with the primary fault during the penultimate event at 2 ka. In addition, the fault model of the Miyaji faults from the inversion modeling in InSAR analysis showed that the slip was limited to areas

shallower than 1.5 km deep. Considering the 2016 event and paleoseismic studies of the primary and secondary faults, the Miyaji faults were activated by triggering from large earthquakes on the adjacent HSRAF (Futagawa fault), and are classified as fully aseismic type. Surface ruptures similar to those observed in the Miyaji area also appeared in other areas surrounding the Futagawa fault during the 2016 event. Therefore, some or most of them may fall into the same category as Miyaji faults (fully aseismic type). These speculations point to the need to reevaluate the seismic hazards of LSRAFs in terms of the frequency and displacement, reminding us that we do not have a proper understanding of LSRAFs. In addition, field evidence of paleo-slips on LSRAFs should be collected in future investigations.

#### Supplementary Information

The online version contains supplementary material available at <https://doi.org/10.1186/s40623-021-01371-x>.

**Additional file 1: Fig. S1.** Photograph showing the relationship between the trench and pit excavations. **Figure S2** Calculated probability distribution of OJS tephra based on OxCal software. **Figure S3** Calculated probability distribution of the penultimate event based on OxCal software.

#### Abbreviations

ACP1: Aso central cone pumice 1; DEM: Digital elevation model; GSI: Geospatial Information Authority of Japan; HGS: Handy Geoslicer; HSRAF: High-slip-rate active fault; InSAR: Interferometric synthetic aperture radar; KS: Kishimadake scoria; LSRAF: Low-slip-rate active fault; N2S: Nakadake N2 scoria; OJS: Ojodake scoria; SfM-MVS: Structure-from-Motion and Multi-View Stereo.

#### Acknowledgements

We thank Yasuo Miyabuchi for the discussion about tephra and Yuichi Kato for help in the trench survey. We used the PALSAR and PALSAR-2 data shared among the PALSAR Interferometry Consortium to Study our Evolving Land Surface (PIXEL), provided by the Japan Aerospace Exploration Agency (JAXA) under a cooperative research contract with the Earthquake Research Institute of the University of Tokyo. The thoughtful comments from the reviewers Hisao Kondo, Rob Langridge and the two anonymous reviewers improved the article.

#### Authors' contributions

DI organized the trench survey, conducted tephra analysis, and drafted the manuscript. DI, HT, YK, NT, TI, and KT conducted the trench survey and drilling surveys and discussed the interpretation of trench walls in the field. ST and NT discussed the behavior of the active faults in Miyaji. YF conducted InSAR analysis. All authors read and approved the final manuscript.

#### Funding

This work was supported by JSPS KAKENHI Grant Number JP17H04730 and JP18K03795.

#### Availability of data and materials

Correspondence and requests for materials should be addressed to DI.

#### Competing interests

The authors declare that they have no competing interests.

#### Author details

<sup>1</sup> Department of Geography, Tokyo Metropolitan University, 1-1, Minami-Osawa, Hachioji, Tokyo 192-0397, Japan. <sup>2</sup> Department of Environmental Systems Science, Faculty of Science and Engineering, Doshisha

University, 1-3, Tataramiyakodani, Kyotanabe, Kyoto 610-0394, Japan. <sup>3</sup> International Research Institute of Disaster Science, Tohoku University, 468-1, Aoba, Aoba-ku, Sendai, Miyagi 980-8572, Japan. <sup>4</sup> Graduate School of Humanities and Social Sciences, Hiroshima University, 1-1-1, Kagamiyama, Higashi-Hiroshima, Hiroshima 739-8524, Japan. <sup>5</sup> Department of Earth Science, Tohoku University, 468-1, Aoba, Aoba-ku, Sendai, Miyagi 980-8572, Japan. <sup>6</sup> Sedimentary Environments Research, 715, Fukae, Nijo, Itoshima, Fukuoka 819-1601, Japan. <sup>7</sup> Fukken Co., Ltd., 3-8-15, Iwamoto-cho, Chiyoda-ku, Tokyo 101-0032, Japan.

Received: 18 June 2020 Accepted: 25 January 2021

Published online: 08 February 2021

## References

- Aoki K (2008) Revised age and distribution of ca. 87 ka Aso-4 tephra based on new evidence from the northwest Pacific Ocean. *Quat Int* 178:100–118. <https://doi.org/10.1016/j.quaint.2007.02.005>
- Asada T (1991) Some questions on active faults. *Acta Fault Res* 9:1–3 (in Japanese)
- Aso City Board of Education (2011) Miyayama ruins II, Cultural property investigation report of Aso City 2. Aso City Board of education, Aso City (in Japanese)
- Bronk Ramsey C (2008) Deposition models for chronological records. *Quat Sci Rev* 27:42–60. <https://doi.org/10.1016/j.quascirev.2007.01.019>
- Bronk Ramsey C (2009) Bayesian Analysis of Radiocarbon Dates. *Radiocarbon* 51:337–360. <https://doi.org/10.1017/S0033822200033865>
- Danhara T, Yamashita T, Iwano H, Kasuya M (1992) An improved system for measuring refractive index using the thermal immersion method. *Quat Int* 13–14:89–91. [https://doi.org/10.1016/1040-6182\(92\)90013-R](https://doi.org/10.1016/1040-6182(92)90013-R)
- Fialko Y, Sandwell D, Agnew D et al (2002) Deformation on nearby faults induced by the 1999 Hector Mine earthquake. *Science* 297:1858–1862. <https://doi.org/10.1126/science.1074671>
- Fujiwara S, Morishita Y, Nakano T et al (2017) Non-tectonic liquefaction-induced large surface displacements in the Aso Valley, Japan, caused by the 2016 Kumamoto earthquake, revealed by ALOS-2 SAR. *Earth Planet Sci Lett* 474:457–465. <https://doi.org/10.1016/j.epsl.2017.07.001>
- Fujiwara S, Yarai H, Kobayashi T et al (2016) Small-displacement linear surface ruptures of the 2016 Kumamoto earthquake sequence detected by ALOS-2 SAR interferometry. *Earth Planets Space* 68:160. <https://doi.org/10.1186/s40623-016-0534-x>
- Fukushima Y, Ishimura D (2020) Characteristics of secondary-ruptured faults in the Aso Caldera triggered by the 2016 Mw7.0 Kumamoto earthquake. *Earth Planets Space* 72:175. <https://doi.org/10.1186/s40623-020-01306-y>
- Fukushima Y, Toda S, Miura S et al (2018) Extremely early recurrence of intraplate fault rupture following the Tohoku-Oki earthquake. *Nat Geosci* 11:777–781. <https://doi.org/10.1038/s41561-018-0201-x>
- Furusawa A, Umeda K (2000) Tephra stratigraphy of piston cores in Beppu Bay during the past 7000 years—correlation of the core tephra with Aso and Kuju Volcano-. *Jour Geol Soc Japan* 106:31–49 (in Japanese with English abstract)
- Goto H, Tsutsumi H, Toda S, Kumahara Y (2017) Geomorphic features of surface ruptures associated with the 2016 Kumamoto earthquake in and around the downtown of Kumamoto City, and implications on triggered slip along active faults. *Earth Planets Space* 69:26. <https://doi.org/10.1186/s40623-017-0603-9>
- Headquarters for Earthquake Research Promotion (2013) Long-term evaluation of the Futagawa and Hinagu fault zones (partial revision version). (in Japanese). [http://www.jishin.go.jp/main/chousa/13feb\\_chi\\_kyushu/k\\_11.pdf](http://www.jishin.go.jp/main/chousa/13feb_chi_kyushu/k_11.pdf). Accessed 29 May 2016
- Imazumi T, Miyauchi T, Tsutsumi H, Nakata T (eds) (2018) Digital active fault map of Japan [Revised Edition]. University of Tokyo Press, Tokyo (in Japanese)
- Ishimura D (2019) Co-seismic vertical displacement associated with the 2016 Kumamoto earthquake (Mw7.0) and activity of the Futagawa fault around Futa, Nishihara Village. *Kumamoto prefecture Act Fault Res* 50:33–44 (in Japanese with English abstract)
- Ishimura D, Toda S, Ichihara T et al (2017) A study on surface ruptures around Miyaji, Aso City, Kumamoto Prefecture, associated with the 2016 Kumamoto earthquake sequence and upward slip tapering on pit excavation walls. *Acta Fault Res* 47:9–16 (in Japanese with English abstract)
- Ishimura D, Toda S, Mukoyama S et al (2019) 3D surface displacement and surface ruptures associated with the 2014 Mw 6.2 nagano earthquake using differential lidar. *Bull Seismol Soc Am* 109:780–796. <https://doi.org/10.1785/0120180020>
- Kamata H, Kodama K (1994) Tectonics of an arc-arc junction: an example from Kyushu Island at the junction of the Southwest Japan Arc and the Ryukyu Arc. *Tectonophysics* 233:69–81. [https://doi.org/10.1016/0040-1951\(94\)90220-8](https://doi.org/10.1016/0040-1951(94)90220-8)
- Komura K, Aiyama K, Nagata T et al (2019) Surface rupture and characteristics of a fault associated with the 2011 and 2016 earthquakes in the southern Abukuma Mountains, northeastern Japan, triggered by the Tohoku-Oki earthquake. *Earth Planets Space* 71:1–23. <https://doi.org/10.1186/s40623-019-1085-8>
- Kumahara Y, Research Group of Inter-University (2016) The characteristics of surface rupture associated by the 2016 Kumamoto Earthquake. Programme and abstracts JSAF 2016 fall meeting, Hosei University, Tokyo, 29–30 October 2016. (in Japanese)
- Kumahara Y, Okada S, Kagohara K et al (2017a) 1:25,000 Active Fault Map, Futagawa-Hinagu Fault Zone and its vicinity “Kumamoto (revision):” Geospatial Information Authority of Japan, Ibaraki (in Japanese)
- Kumahara Y, Torii M, Nakata T, et al (2017) Fault history of the northern part of Futagawa-Hinagu fault zone based on trench survey at Dozon, Mashiki Town and at Kawayo, Minami-Aso Village, Programme and abstracts JSAF 2017 fall meeting, Hiroshima University, Higashi-Hiroshima, 24–25 November 2017 (in Japanese)
- Kumamoto Prefectural Board of Education (2010) Earthquake traces in Onobaru-A site. Onobaru ruins group. Cultural property investigation report of Kumamoto Pref 257 (2), 147–159. (in Japanese).
- Maruyama T, Yoshimi M, Saito E, Saito M (2014) Examination of fault activity of the surface ruptures associated with the April 11, 2011 Fukushima Hamadori earthquake (MJMA 7.0) based on tectonic geomorphic and paleoseismic surveys. In: Research Planning Office for Geological Survey and Applied Geoscience (ed) Reports of Research and Investigation on Multiple Geological Hazards Caused by Huge Earthquakes. *GSJ Interim Rep* 66:125–136. (in Japanese with English abstract).
- Matsumoto Y (1979) Some problems on volcanic activities and depression structures in Kyushu, Japan. *Mem Geol Soc Japan* 16:127–139 (in Japanese with English abstract)
- Miyabuchi Y (2009) A 90,000-year tephrostratigraphic framework of Aso Volcano, Japan. *Sediment Geol* 220:169–189. <https://doi.org/10.1016/j.sedgeo.2009.04.018>
- Miyabuchi Y (2017) Eruption history of Janoo volcano in the northwestern part of Aso caldera, Japan. *Bull Volcanol Soc Japan* 62:1–12 (in Japanese with English abstract)
- Miyabuchi Y, Watanabe K (1997) Eruption ages of Holocene tephra from Aso volcano, southwestern Japan, inferred from <sup>14</sup>C Ages of buried Andisols. *Bull Volcanol Soc Japan* 42:403–408 (in Japanese with English abstract)
- Miyashita Y (2018) Holocene paleoseismic history of the Yunodake fault ruptured by the 2011 Fukushima-ken Hamadori earthquake, Fukushima Prefecture, Japan. *Geomorphology* 323:70–79. <https://doi.org/10.1016/j.geomorph.2018.08.040>
- Moya L, Yamazaki F, Liu W, Chiba T (2017) Calculation of coseismic displacement from lidar data in the 2016 Kumamoto, Japan, earthquake. *Nat Hazards Earth Syst Sci* 17:143–156. <https://doi.org/10.5194/nhess-17-143-2017>
- Nakata T, Imaizumi T (eds) (2002) Digital active fault map of Japan. University of Tokyo Press, Tokyo (in Japanese)
- Nakata T, Shimazaki K (1997) Geo-slicer, a newly invented soil sample, for high-resolution active fault studies. *Jour Geogr* 106:59–69 (in Japanese with English abstract)
- Nishimura T, Tobita M, Yarai H et al (2008) Episodic growth of fault-related fold in northern Japan observed by SAR interferometry. *Geophys Res Lett* 35:1–5. <https://doi.org/10.1029/2008GL034337>
- Okada S, Ishimura D, Niwa Y, Toda S (2015) The first surface-rupturing earthquake in 20 years on a HERP active fault is not characteristic: The 2014 Mw 6.2 Nagano event along the northern Itoigawa-Shizuoka tectonic line. *Seismol Res Lett* 86:1287–1300. <https://doi.org/10.1785/0220150052>
- Okamura Y, Abe S, Miyashita Y, et al (2018) 3.1 Survey of detailed position and shape of active faults to understand the fault segments and observation to reveal the paleoseismic history and slip rates. In: Research report of a comprehensive active fault survey after the 2016 Kumamoto earthquake,



- 2017 fiscal year. Ministry of Education, Culture, Sports, Science and Technology and Kyushu University. (in Japanese) [https://www.jishin.go.jp/main/chousakenkyuu/kumamoto\\_sogochousa/h29/h29kumamoto\\_sogochousa\\_3\\_1.pdf](https://www.jishin.go.jp/main/chousakenkyuu/kumamoto_sogochousa/h29/h29kumamoto_sogochousa_3_1.pdf). Accessed 29 May 2016
- Ono K, Watanabe K (1985) Geological map of Aso Volcano. Geological map of volcanoes, Geological Survey of Japan, Tsukuba **(in Japanese)**
- Price EJ, Sandwell DT (1998) Small-scale deformations associated with the 1992 Landers, California, earthquake mapped by synthetic aperture radar interferometry phase gradients. *J Geophys Res Solid Earth* 103:27001–27016. <https://doi.org/10.1029/98jb01821>
- Reimer PJ, Edouard Bard B, Alex Bayliss B et al (2013) Intcal13 and Marine13 Radiocarbon Age Calibration Curves 0–50,000 Years Cal Bp. *Radiocarbon* 55:1869–1887. <https://doi.org/10.1017/S0033822200048864>
- Research Group for Active Faults of Japan (1980) Active Faults in Japan, sheet maps and inventories. University of Tokyo Press, Tokyo **(in Japanese)**
- Research Group for Active Faults of Japan (1991) Active Faults in Japan, sheet maps and inventories, rev. University of Tokyo Press, Tokyo **(in Japanese)**
- Saito H, Uchiyama S, Hayakawa YS, Obanawa H (2018) Landslides triggered by an earthquake and heavy rainfalls at Aso volcano, Japan, detected by UAS and SfM-MVS photogrammetry. *Prog Earth Planet Sci* 5:1–10. <https://doi.org/10.1186/s40645-018-0169-6>
- Scott CP, Arrowsmith JR, Nissen E et al (2018) The M7 2016 Kumamoto, Japan, Earthquake: 3-D Deformation Along the Fault and Within the Damage Zone Constrained From Differential Lidar Topography. *J Geophys Res Solid Earth* 123:6138–6155. <https://doi.org/10.1029/2018JB015581>
- Shimazaki K (2008) Long-term forecast of large earthquakes on active faults in Japan: estimation of earthquake frequency. *Acta Fault Res* 28:41–51 **(in Japanese with English abstract)**
- Shirahama Y, Yoshimi M, Awata Y et al (2016) Characteristics of the surface ruptures associated with the 2016 Kumamoto earthquake sequence, central Kyushu. *Japan Earth Planets Space* 68:191. <https://doi.org/10.1186/s40623-016-0559-1>
- Smith VC, Staff RA, Blockley SPE et al (2013) Identification and correlation of visible tephra in the Lake Suigetsu SG06 sedimentary archive, Japan: Chronostratigraphic markers for synchronising of east Asian/west Pacific palaeoclimatic records across the last 150 ka. *Quat Sci Rev* 67:121–137. <https://doi.org/10.1016/j.quascirev.2013.01.026>
- Suzuki Y, Ishimura D, Kumaki Y et al (2017) 1:25,000 Active Fault Map, Futagawa-Hinagu Fault Zone and its vicinity "Aso." Geospatial Information Authority of Japan, Ibaraki **(in Japanese)**
- Tajima Y, Hasenaka T, Torii M (2017) Effects of the 2016 Kumamoto earthquakes on the Aso volcanic edifice. *Earth Planets Space* 69:63. <https://doi.org/10.1186/s40623-017-0646-y>
- Takada K, Nakata T, Miyagi T et al (2002) Handy Geoslicer – new soil sampler for Quaternary geologist. *Chishitsu News* 579:12–18 **(in Japanese)**
- Takahashi N, Ishimura D, Toda S et al (2017) Vertical slip rate on a normal fault co-ruptured with the Futagawa fault at the 2016 Kumamoto earthquake. *Acta Fault Res* 46:27–32 **(in Japanese with English abstract)**
- Toda S, Ishimura D (2019) Evaluation of short active faults reflected from distributed minor surface breaks found at recent inland large earthquakes including the 2016 Kumamoto earthquake. *Quatern Res* 58:121–136 **(in Japanese with English abstract)**
- Toda S, Tsutsumi H (2013) Simultaneous reactivation of two, subparallel, inland normal faults during the Mw 6.6 11 April 2011 Iwaki earthquake triggered by the Mw 9.0 Tohoku-oki, Japan. *Earthquake Bull Seismol Soc Am* 103:1584–1602. <https://doi.org/10.1785/0120120281>
- Toda S, Kaneda H, Okada S et al (2016) Slip-partitioned surface ruptures for the Mw 7.0 16 April 2016 Kumamoto, Japan, earthquake. *Earth Planets Space* 68:188. <https://doi.org/10.1186/s40623-016-0560-8>
- Toda S, Torii M, Okuno M et al (2019) Evidence for Holocene paleoseismic events on the 2016 Kumamoto earthquake rupture zone within the Aso caldera: A trench excavation survey at Kurokawa, the town of Minami-Aso, southwest Japan. *Acta Fault Res* 51:13–25 **(in Japanese with English abstract)**
- Tsuji T, Ishibashi J, Ishitsuka K, Kamata R (2017) Horizontal sliding of kilometre-scale hot spring area during the 2016 Kumamoto earthquake. *Sci Rep* 7:42947. <https://doi.org/10.1038/srep42947>
- Tsutsumi H, Toda S, Goto H et al (2018) Paleoseismic trenching across the surface rupture of the 2016 Kumamoto earthquake at Jichu, Mashiki Town, Kumamoto Prefecture. *Acta Fault Res* 49:31–39 **(in Japanese with English abstract)**
- Ueta K, Miyawaki R, Iemura K, et al (2018) Paleoseismological study on surface fault ruptures produced by the 2016 Kumamoto earthquake. Abstracts of Japan Geoscience Union Meeting 2018, Makuhari Messe, Chiba, 20–24 May 2018 (in Japanese with English abstract)
- Une H, Nakano T, Sato H, et al (2019) Past activity of 'triggered fault' in the northwest of outer rim of Aso caldera estimated from the results of excurvation survey and displacement topography. Abstracts of Japan Geoscience Union Meeting 2019, Makuhari Messe, Chiba, 26–30 May 2019 (in Japanese with English abstract)
- Wei M, Sandwell D, Fialko Y, Bilham R (2011) Slip on faults in the Imperial Valley triggered by the 4 April 2010 Mw 7.2 El Mayor-Cucapah earthquake revealed by InSAR. *Geophys Res Lett* 38:1–6. <https://doi.org/10.1029/2010GL045235>
- Wright T, Fielding E, Parsons B (2001) Triggered slip: Observations of the 17 August 1999 Izmit (Turkey) earthquake using radar interferometry. *Geophys Res Lett* 28:1079–1082. <https://doi.org/10.1029/2000GL011776>
- Yamada K, Takemura K, Kuwae M et al (2017) Revised ages of late Holocene tephra in Beppu Bay, central Kyushu, southwest Japan. *Quat Int* 452:33–42. <https://doi.org/10.1016/j.quaint.2017.01.024>

## Publisher's Note

Springer Nature remains neutral with regard to jurisdictional claims in published maps and institutional affiliations.

Submit your manuscript to a SpringerOpen® journal and benefit from:

- Convenient online submission
- Rigorous peer review
- Open access: articles freely available online
- High visibility within the field
- Retaining the copyright to your article

Submit your next manuscript at ► [springeropen.com](https://www.springeropen.com)